Splay faults imaged by fluid-driven aftershocks of the 2004 M_w 9.2 Sumatra-Andaman earthquake

Felix Waldhauser[1], David P. Schaff[1], Tobias Diehl[1], and E. Robert Engdahl[2]
[1]Lamont-Doherty Earth Observatory, Columbia University, Palisades, New York 10964, USA
[2]Department of Physics, University of Colorado at Boulder, Boulder, Colorado 80309-0390, USA

ABSTRACT

High-precision teleseismic double-difference locations and focal mechanisms of aftershocks of the A.D. 2004 M_w 9.2 Sumatra-Andaman earthquake illuminate an active imbricate fault system in the accretionary prism offshore northern Sumatra. They reveal repeated failure of a shallow northeast-dipping thrust fault above the megathrust, which we interpret to be the reactivation of a splay fault that rises from the megathrust at ~55 km depth and cuts through the overriding Sunda plate. The projected intersection of the splay fault with the seafloor correlates with a recently active thrust fault seen in postseismic bathymetry data west of the Aceh basin. A spatiotemporal analysis of the streaky aftershock distribution indicates that ascending fluids released from the subducting oceanic crust along inherited seafloor fabric may control brittle fracture in the overriding plate. We speculate that if the splay fault was active coseismically, it may have led to amplified vertical uplift of the forearc ridge and contributed to generating the cataclysmic near-field tsunami that struck the northwest Sumatra coast following the 2004 rupture.

INTRODUCTION

Great earthquakes and tsunamis along subduction zones are generated when large areas of the megathrust rupture and slip propagates along faults, transferring displacement close to the seafloor. The tsunamogenic effect can be amplified when coseismic slip occurs along splay faults that rise from the plate boundary megathrust and intersect the seafloor at a steep angle. Splay faults have been shown to play important roles in accommodating elastic strain in great subduction earthquakes in Alaska, United States (Plafker, 1972), and Japan (e.g., Strasser et al., 2009), and in the generation of large tsunamis (e.g., Fukao, 1979). However, results from the A.D. 2011 Tohoku, Japan (M_w 9.0), earthquake and tsunami indicate that significant displacement may have occurred along the megathrust all the way to the trench (Lay et al., 2011).

The M_w 9.2 Sumatra-Andaman megathrust earthquake of 26 December 2004 generated a massive tsunami that caused devastation throughout the Indian Ocean (Lay et al., 2005). Despite significant earthquakes along the Sunda subduction zone in the past (Newcomb and McCann, 1987), the structure and morphology of this plate boundary system and its potential for generating large tsunamis are poorly understood. Understanding these issues is particularly timely because of the increased activity of this subduction zone since 2004. Here we combine four years of high-resolution teleseismic aftershock relocations and focal mechanisms to illuminate seismogenesis and active faults in the accretionary prism offshore northern Sumatra.

DATA AND METHODS

Following the 2004 mainshock, a localized cluster of intense aftershock activity occurred offshore Banda Aceh in northern Sumatra, ~200 km east of the Sunda Trench, where the Indo-Australian plate underthrusts the Sunda plate at a rate of 52 mm/yr (Sieh and Natawidjaja, 2000) (Fig. 1B). The aftershocks also locate beneath the Aceh basin, which is bounded on its western border by the NNW-striking, right-lateral West Andaman fault. They occur downdip of a change in trend of the Sunda Trench and beneath a change in trend of the West Andaman fault that cuts through the forearc, suggesting that the distortion of the plate interface at depth may have created a barrier to mainshock rupture propagation, leaving the intraplate thrust offshore Banda Aceh unbroken (Dewey et al., 2007). Coseismic slip models based on planar faults (e.g., Chlieh et al., 2007) indicate very small displacement (few meters or less) along the megathrust in the area of the aftershock cluster, surrounded updip and to the south by high displacements (~16 m). Aftershocks recorded in the offshore Banda Aceh area by short-term ocean bottom seismometer deployments were interpreted to locate primarily on the plate interface, with little activity in the overriding plate (Araki et al., 2006; Sibuet et al., 2007; Lin et al., 2009).

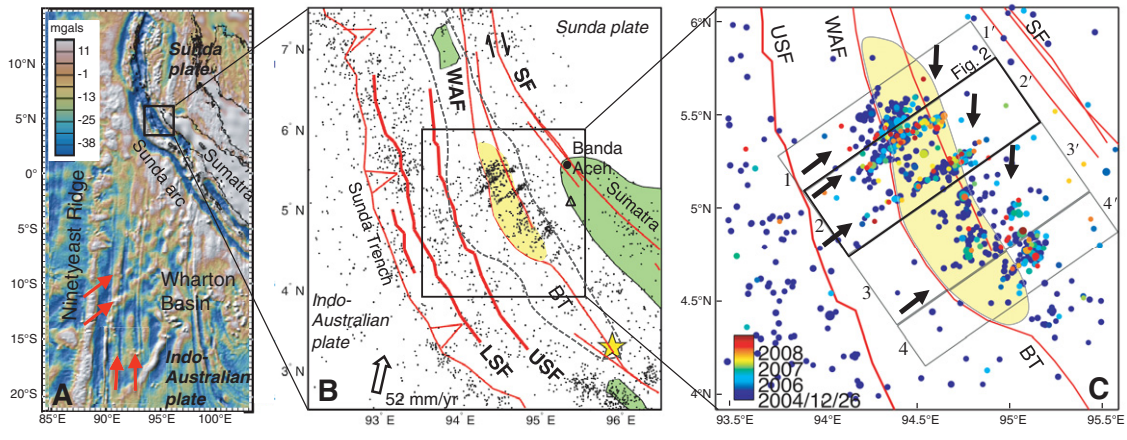

Figure 1. A: Free-air gravity anomalies (Sandwell and Smith, 1997) draped over bathymetric relief of Sunda arc (Indonesia). Red arrows indicate orientation of fracture zones. B: Overview of study area. Gray dots are relocated aftershock epicenters; yellow star denotes 2004 M_w 9.2 mainshock; yellow area outlines Aceh basin; dashed line encloses estimated tsunami source region (Lay et al., 2005); triangle denotes global positioning system station UMLH; red lines are faults. WAF—West Andaman fault; BT—back thrust; SF—Sumatra fault; USF—upper splay fault; LSF—lower splay fault (Lin et al., 2009). Convergence information from Sieh and Natawidjaja (2000). C: Map view of relocated earthquakes offshore Banda Aceh, color coded by year of occurrence. Black annotated rectangles include events shown in depth sections in Figure 2 and Figure DR1 (see footnote 1). Arrows indicate northeast- and north-northeast orientation of selected streaks.

We relocated 1191 earthquakes that occurred between 1964 and 2008 in the offshore Banda Aceh region by applying teleseismic cross-correlation and double-difference methods (Waldhauser and Schaff, 2007) to global earthquake bulletin data (International Seismological Centre, UK, 1964–2006; U.S. Geological Survey Earthquake Data Report, 2007–2008) and waveform data (International Research Institution for Seismology). More than 1.7×10^6 first and later-arriving teleseismic phase pick delay times between nearby events at common stations, and 113,000 high-precision cross-correlation measurements for P, PKP, S, and SKS phases, are inverted for relative hypocenter locations. Approximately 50% of the events share correlated seismograms with at least one other event with a correlation coefficient ≥0.8 at one or more stations, indicating similar location and focal mechanisms.

A new multistep relocation procedure is used to improve on the large errors in standard global catalog locations. We employ a single-event double-difference algorithm (Waldhauser, 2009) to relocate each event in the International Seismological Centre and U.S. Geological Survey Earthquake Data Report catalogs relative to a subset of accurately located hypocenters computed using depth phases (Engdahl et al., 2007). The improved initial locations are then used in a simultaneous double-difference inversion of the combined pick and correlation delay times. The final double-difference locations have average root mean square (RMS) residuals of 0.341 s (initial RMS = 0.693 s) for the bulletin picks and 0.053 s for the cross-correlation data. Relative location uncertainties at the 95% confidence level derived from a bootstrap analysis have medians of 2.5 km laterally and 1.8 km vertically. We used a grid search procedure together with a regional three-dimensional (3-D) velocity model (Widiyantoro and Van der Hilst, 1996) to find that the absolute location bias in our study area is <3 km.

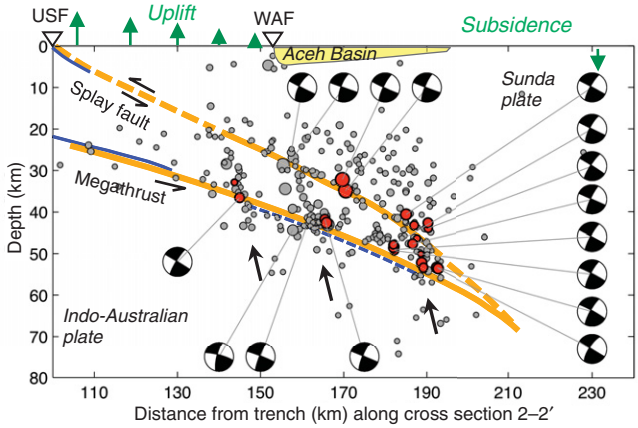

Figure 2. Depth distribution of hypocenters (gray and red dots) along section 2–2′ (see Fig. 1C for location). No vertical exaggeration. Circle size scales with magnitude (range: M_w 2.2–6.2). Global centroid moment tensor double-couple focal mechanisms are shown in cross-sectional view. Red dots denote repeating earthquakes with highly correlated seismograms; triangles mark locations of faults mapped at surface; orange lines show position of plate interface and master splay fault inferred in this study (dashed: projected); blue solid lines show projected positions of top oceanic crust and shallow northeast-dipping fault inferred from active-source data (Chauhan et al., 2009); blue dashed line shows plate interface inferred from limited local passive-source data (Araki et al., 2006; Sibuet et al., 2007); green arrows represent observed uplift or subsidence based on coseismic data and 1 month of postseismic geodetic data (Chlieh et al., 2007). Black arrows point to inferred fluid pathways. USF—upper splay fault (Lin et al., 2009); WAF—West Andaman fault.

IMBRICATE FAULT SYSTEM

The relocated aftershocks occur in a region of little pre-shock activity (392 events over 50 yr), comparable to other areas along the subduction zone. The general pattern of the aftershock distribution shows northeast-oriented lineations (or streaks) as much as 80 km long and only a few kilometers wide, separated by sparsely seismic zones (Figs. 1B and 1C). The two most prominent streaks occur in the northern part of the study area. Some sections of the streaks are formed by short, NNE-striking features, or substreaks. In the southern part of the study area, south of 5°N, the streaks are shorter, their epicentral distribution is broader, but their orientations are still predominately northeast and north-northeast trending.

A northeast-oriented cross section along 2–2′ (see Fig. 1C for location), including the two dominant streaks, indicates that the majority of hypocenters occur both on or near the plate interface and throughout the overriding Sunda plate (Fig. 2; Fig. DR1 in the GSA Data Repository[1]). The position of the plate interface, as inferred from the relocated seismicity, steepens from 10° at the Sunda trench to ~30° beneath the eastern border of the Aceh basin. Our interface position is consistent with the plate geometry of Hayes and Wald (2009) for the offshore Banda Aceh region and with reflection data collected north of our study area (Chauhan et al., 2009) (Fig. 2). Earthquakes above the plate interface are generally smaller and more broadly distributed. Between ~20 and 50 km depth, they form steeply northeast-dipping structures that appear to rise from the plate interface (arrows in Fig. 2).

Global centroid moment tensor solutions show predominately thrust motion on planes striking northwest parallel to the trench and perpendicular to the orientation of the streaks (Fig. 2; Fig. DR1). Assuming that the shallowly northeast-dipping nodal plane is the active fault plane, fault dips for events along the plate interface continuously increase from ~15° on the trench side of the cross section to ~33° near the downdip extent of the seismogenic megathrust, consistent with the deepening slab interface inferred from the relocated seismicity. Focal mechanisms of events above the plate interface also show northeast-dipping thrust mechanisms.

Our results suggest that most aftershocks represent thrust motion on the plate interface and on northwest-striking imbricate faults that cut through the accretionary wedge. In particular, we infer the position of a master splay from several larger aftershocks that locate above the plate interface and indicate shallow thrust motion along a northeast-dipping fault (Fig. 2; Fig. DR1). The inferred master splay branches off the plate interface at ~55 km depth and 190 km from the trench and cuts through the forearc to an inferred surface location at the western border of the forearc ridge, ~100 km from the trench. Events above the master splay indicate distributed deformation and do not appear to occur on long faults.

Repeating events with strongly correlated seismograms (red dots in Fig. 2 and Fig. DR1) occur either on the megathrust or on the master splay fault, with the highest concentrations observed near the downdip end of the seismogenic megathrust, between 50 and 60 km depth. These events may mark repeated slip on faults controlled by stress concentrations at the transition from seismic (updip) to aseismic (downdip) slip. The observed curvature in the slab interface at this location may facilitate the initiation of the master splay fault. Highly correlated aftershocks in the overriding plate suggest repeated thrust failure of the master splay fault and thus support the idea of a reactivation of a more mature imbricate fault system in this area.

AFTERSHOCK STREAKS

Because of the lack of strike-slip movement on the near-vertical planes of seismicity, we can rule out strain partitioning as the primary cause of brittle failure along the streaks of earthquakes in the overrid-

[1]GSA Data Repository item 2012062, Figure DR1 (hypocenter depth-sections 1 to 4) and Table DR1 (fluid flow rates, correlation coefficients, and p-values for periods 1 to 5), is available online at www.geosociety.org/pubs/ft2012.htm, or on request from editing@geosociety.org or Documents Secretary, GSA, P.O. Box 9140, Boulder, CO 80301, USA.

ing plate. The striking similarity between the orientation of the aftershock streaks (59°–63°NW and ~5°N) (Fig. 1C) and the fracture orientation offshore in the Wharton Basin of the Indian plate (~64°NW and 3°–6°N) (Fig. 1A) suggests that fluids may play an important role in the generation of the earthquakes. The fluids may be expelled into the overriding plate from water-rich fractures in the oceanic crust that were formed more than 5 m.y. ago (assuming a constant subduction rate of 52 mm/yr), presumably by pore collapse during slip on the plate interface. As the fluids move upward, preferably along preexisting weak zones within the overriding plate, they may cause earthquakes by lowering the frictional strength on imbricate faults that have built up strains to near the failure level.

In the Wharton Basin, northwest-southeast-oriented main compressive stresses (Delescluse and Chamot-Rooke, 2007) cause large-scale undulations of the basin lithosphere that can be seen in free-air gravity maps (Fig. 1A). The buckling of the plate produces northeast-southwest–oriented fractures near the surface of the oceanic crust (Weissel et al., 1980), generating pathways for fluids to hydrate the fracture zones. Similarly, fluids along the north-south–oriented streaks may have entered the oceanic crust by reactivation and hydration of north-south-oriented paleotransform faults (Fig. 1A) that are part of the fossil Wharton ridge. Hydration of the bending-controlled fractures on the seafloor is more efficient than along the transform faults because of their extensional character, which might explain the dominance of northeast-southwest-oriented aftershock lineations (Fig. 1C).

To test the hypothesis of fluid driven aftershocks we plot the distance of hypocenters to the plate interface as a function of time (black dots, Fig. 3A). The distribution is shown for 3 time intervals: first month after the mainshock (left panel), months 2–10 (center), and months 11–50 (right). Mean depths (gray dots) within bins of 2, 14, and 60 days of data, respectively, indicate at least 5 robust periods with clear trends of ascending hypocenters, separated by short periods of steeply declining depths. We estimate the rate of fluid flow as expressed by the ascending hypocenters by a least square fit (black lines, Fig. 3A) of all data within each of the 5 periods, yielding significant (p-values <0.03) correlation coefficients between 0.25 and 0.36 (Table DR1). Fluid flow rates decrease exponentially from 612 m/day 12 days after the mainshock to 23 m/day 3 yr later (Fig. 3B). We obtain similar flow rates when considering only earthquakes along the two streaks (dashed lines in Fig. 3; Table DR1).

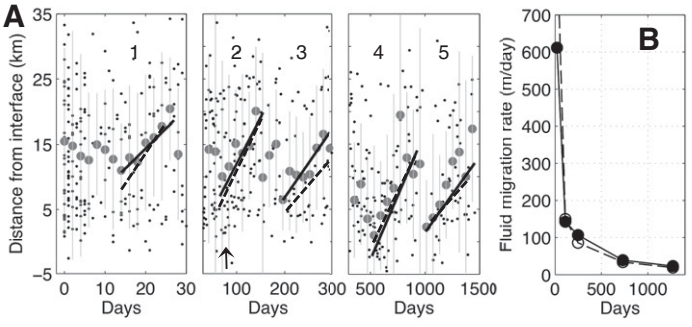

Figure 3. A: Time of aftershocks as function of distance from plate interface (small black dots) for 3 time intervals: days 0–30 after mainshock (left), days 30–300 (center), and days 300–1500 (right). Large gray dots are mean depths within bins of 2 (left), 14 (center), and 60 days (right) and are used to guide in identification of fluid flow periods 1–5. Thin gray lines are associated standard deviations. Black solid lines are least squares fit to all earthquakes (i.e., black dots) within each of five inferred fluid flow periods (1–5); dashed lines are least squares fit only to earthquakes along section 2–2′. Correlation coefficients are between 0.25 and 0.36 with p-values <0.03, except for period 5 (see Table DR1 [see footnote 1]). Arrow denotes occurrence of M_w 8.6 Nias Island (Indonesia) earthquake (28 March 2005). B: Fluid flow rates taken from least squares fits in A plotted as function of days (mean of each period) after mainshock. Solid line represents all events; dashed line represents only those along section 2–2′ (Fig. 2).

Given the fluid flow rates we can estimate the permeabilities, κ, of the overriding plate by solving the one-dimensional diffusion equation:

$$\kappa = \left(\phi\beta_f + \phi\beta_r\right)\eta l^2/\tau, \quad (1)$$

where l is the length scale of the process and τ is its duration, β_f and β_r are the fluid and rock compressibilities, respectively, ϕ is the rock porosity, and η is the fluid viscosity. For low-porosity rocks ($\phi < 0.02$) at 150 °C, where $\beta_f = 5 \times 10^{-10}$ Pa^{-1}, $\beta_r = 2 \times 10^{-11}$ Pa^{-1}, and $\eta = 1.9 \times 10^{-4}$ Pa·s (Townend and Zoback, 2000), we obtain permeabilities in the range of 2.5×10^{-10} to 2.5×10^{-13} m^2. These are several orders of magnitudes larger than permeabilities for intraplate crust (Townend and Zoback, 2000) and accretionary wedges elsewhere in the world (Koerner et al., 2004). However, the reactivated network of imbricate faults is likely to provide highly permeable pathways for fluids released from the subducting slab. Furthermore, as suggested by the exponential decay of fluid flow rate with time (Fig. 3B), the extent and magnitude of shaking during the main shock may have temporarily increased permeability.

The robustness of timing and rate of the inferred fluid movement across the offshore Banda Aceh area suggest that fluid release may be controlled by regionally acting processes such as afterslip. The global positioning system station UMLH (Fig. 1B) in northern Sumatra recorded one of the largest postseismic southwest-directed displacements along the entire plate boundary (75 cm during the first month). However, the data are too noisy to allow for correlation between deformation and fluid flow events. The onset of fluid flow event 2 (at 90 days, Fig. 3A) correlates with the 28 March 2005 M_w 8.6 Nias Island (Indonesia) earthquake, which occurred 430 km southeast of our study area, suggesting that the release of fluids from the subducting plate may have been dynamically triggered.

DISCUSSION AND CONCLUSION

Our aftershock analysis supports a postseismically active imbricate fault system offshore northern Sumatra that may have also been active coseismically. Although accretionary wedges are often seen as aseismic, large earthquakes may propagate through the shallow low-strength stable zone to the surface (Scholz, 1998). The inferred surface projection of our proposed master splay fault coincides with a recently active northeast-dipping thrust feature seen in swath-bathymetric data collected shortly after the 2004 earthquake and interpreted as a possible splay fault (USF in Figs. 1 and 2; Lin et al., 2009). This fault was also imaged at shallow depths with active-source data (Fig. 2; Chauhan et al., 2009). However, reflection data collected north of our study area show a southwest-dipping backthrust that intersects the seafloor at the northwestern border of the Aceh basin (Chauhan et al., 2009). Singh et al. (2011) argued that the enhanced reflectivity of the backthrust may indicate that it was active coseismically, although they cannot rule out a lithological cause. A reconnaissance cruise along the western border of the Aceh basin, where significant slip along the backthrust would have broken the seafloor, found no major disturbance of the sediment beds (Seeber et al., 2007). Furthermore, swath-bathymetric data (Sibuet et al., 2007) and near-surface active source data (Chauhan et al., 2009) depict a relatively undisturbed forearc ridge east of the upper splay fault.

Because the inferred splay fault reaches the ocean floor at a steeper angle than the plate-boundary interface, coseismic slip on the splay fault during the 2004 event would have caused vertical motion of the adjacent outer arc larger than that resulting from slip on the megathrust alone. Both geodetic data (Chlieh et al., 2007) and satellite imagery (Meltzner et al., 2006) show amplified vertical displacement above the shallow segment of the splay fault and subsidence landward across the Aceh basin (Fig. 2, green arrows). The area of amplified uplift is consistent with the general

location of the source of the tsunami inferred from wave traveltimes (Lay et al., 2005) (Fig. 1B, black dashed line). If coseismic slip occurred on the proposed master splay, it may have contributed to the cataclysmic secondary near-field tsunami that was postulated to have originated near the forearc ridge, based on early tsunami arrival times and high run-up heights (Plafker et al., 2006) and double-peaked lead waves recorded on the transects of the Jason-1 satellite (Smith et al., 2005).

The high-precision aftershock locations presented here reveal active faults in the accretionary wedge offshore northern Sumatra and point to postseismic fluid processes controlling brittle failure. The spatiotemporal details emerged after reducing location uncertainties in standard global earthquake catalogs from tens of kilometers to less than a few kilometers using a teleseismic double-difference procedure, suggesting that teleseismic data may be harnessed to image active faults associated with other recent great subduction earthquakes. Understanding the seismogenic structure of subduction zones is key to resolving the evolution and distribution of coseismic and postseismic slip during great earthquakes and assessing seismic and tsunami hazards.

ACKNOWLEDGMENTS

We thank N. Seeber, A. Malinverno, L. Sykes, and S. Singh for useful discussions, and S. Wyld, C. Sibuet, S. Singh, and three anonymous reviewers for constructive reviews. Supported by the National Science Foundation (grant EAR-06-08739) and the U.S. Geological Survey (G09AP00132). This is Lamont-Doherty Earth Observatory contribution 7500.

REFERENCES CITED

Araki, E., Shinohara, M., Obana, K., Yamada, T., Kameda, Y., Kanazawa, T., and Suyehiro, K., 2006, Aftershock distribution of the December 26, 2004, Sumatra-Andaman earthquake from ocean bottom seismographic observations: Earth, Planets and Space, v. 58, p. 113–119.

Chauhan, A.P.S., Singh, S.C., Hananto, N.D., Carton, H., Klingelhoefer, F., Dessa, J.-X., Permana, H., White, N.J., and Graindorge, D., and the Sumatra OBS Scientific Team, 2009, Seismic imaging of forearc backthrusts at northern Sumatra subduction zone: Geophysical Journal International, v. 179, p. 1772–1780, doi:10.1111/j.1365-246X.2009.04378.x.

Chlieh, M., Avouac, J.-P., Hjorleifsdottir, V., Song, T.R.A., Ji, C., Sieh, K., Sladen, A., Hebert, H., Prawirodirdjo, L., Bock, Y., and Galetzka, J., 2007, Coseismic slip and afterslip of the great M_w 9.15 Sumatra–Andaman earthquake of 2004: Seismological Society of America Bulletin, v. 97, p. S152–S173, doi:10.1785/0120050631.

Delescluse, M., and Chamot-Rooke, N., 2007, Instantaneous deformation and kinematics of the India-Australia plate: Geophysical Journal International, v. 168, p. 818–842, doi:10.1111/j.1365-246X.2006.03181.x.

Dewey, J.W., Benz, H., Choy, G., Earle, P., Presgrave, B., Sipkin, S., Tarr, A.C., and Wald, D., 2007, Seismicity associated with the Sumatra–Andaman Islands earthquake of 26 December 2004: Seismological Society of America Bulletin, v. 97, p. S25–S42, doi:10.1785/0120050626.

Engdahl, E.R., Villasenor, A., DeShon, H.R., and Thurber, C.H., 2007, Teleseismic relocation and assessment of seismicity (1918–2005) in the region of the 2004 M_w 9.0 Sumatra–Andaman and 2005 M_w 8.6 Nias Island great earthquakes: Seismological Society of America Bulletin, v. 97, p. S43–S61, doi:10.1785/0120050614.

Fukao, Y., 1979, Tsunami earthquakes and subduction processes near the deep-sea trenches: Journal of Geophysical Research, v. 84, p. 2303–2314, doi:10.1029/JB084iB05p02303.

Hayes, G.P., and Wald, D.J., 2009, Developing a framework to constrain the geometry of the seismic rupture plane on subduction interfaces a priori—A probabilistic approach: Geophysical Journal International, v. 176, p. 951–964, doi:10.1111/j.1365-246X.2008.04035.x.

Koerner, A., Kissling, E., and Miller, S.A., 2004, A model of deep crustal fluid flow following the M_w =8.0 Antofagasta, Chile, earthquake: Journal of Geophysical Research, v. 109, B06307, doi:10.1029/2003JB002816.

Lay, T., and 13 others, 2005, The great Sumatra–Andaman earthquake of 26 December 2004: Science, v. 308, p. 1127–1133, doi:10.1126/science.1112250.

Lay, T., Ammon, C.J., Kanamori, H., Xue, L., and Kim, M.J., 2011, Possible large near-trench slip during the great 2011 Tohoku (M_w 9.0) earthquake: Earth, Planets and Space, v. 63, doi:10.5047/eps.2011.05.033.

Lin, J.-Y., Le Pichon, X., Rangin, C., Sibuet, J.-C., and Maury, T., 2009, Spatial aftershock distribution of the 26 December 2004 great Sumatra-Andaman earthquake in the northern Sumatra area: Geochemistry Geophysics Geosystems, v. 10, Q05006, doi:10.1029/2009GC002454.

Meltzner, A.J., Sieh, K., Abrams, M., Agnew, D.C., Hudnut, K.W., Avouac, J.-P., and Natawidjaja, D.H., 2006, Uplift and subsidence associated with the great Aceh-Andaman earthquake of 2004: Journal of Geophysical Research, v. 111, B02407, doi:10.1029/2005JB003891.

Newcomb, K.R., and McCann, W.R., 1987, Seismic history and seismotectonics of the Sunda Arc: Journal of Geophysical Research, v. 92, p. 421–439, doi:10.1029/JB092iB01p00421.

Plafker, G., 1972, The Alaskan earthquake of 1964 and Chilean earthquake of 1960; implications for arc tectonics and tsunami generation: Journal of Geophysical Research, v. 77, no. 5, p. 901–925, doi:10.1029/JB077i005p00901.

Plafker, G., Nishenko, S., Cluff, L., and Syahrial, M., 2006, The cataclysmic 2004 tsunami on NW Sumatra—Preliminary evidence for a near-field secondary source along the western Aceh Basin: Seismological Research Letters, v. 77, p. 231.

Sandwell, D.T., and Smith, W.H.F., 1997, Marine gravity anomaly from Geosat and ERS-1 satellite altimetry: Journal of Geophysical Research, v. 102, p. 10039–10054, doi:10.1029/96JB03223.

Scholz, C.H., 1998, Earthquakes and friction laws: Nature, v. 391, p. 37–42, doi:10.1038/34097.

Seeber, L., Mueller, C., Fujiwara, T., Arai, K., Soh, W., Djajadihardja, Y.S., and Cormier, M.H., 2007, Accretion, mass wasting, and partioned strain over the 26 December 2004 Mw9.2 rupture offshore Aceh, northern Sumatra: Earth and Planetary Science Letters, v. 263, p. 16–31, doi:10.1016/j.espl.2007.07.057.

Sibuet, J.-C., and 13 others, 2007, 2004 great Sumatra-Andaman earthquake: Coseismic and post-seismic motions in northern Sumatra: Earth and Planetary Science Letters, v. 263, p. 88–103, doi:10.1016/j.epsl.2007.09.005.

Sieh, K., and Natawidjaja, D., 2000, Neotectonics of the Sumatran fault, Indonesia: Journal of Geophysical Research, v. 105, p. 28,295–28,326, doi:10.1029/2000JB900120.

Singh, S.C., Hananto, N.D., and Chauhan, A.P.S., 2011, Enhanced reflectivity of backthrusts in the recent great Sumatran earthquake rupture zones: Geophysical Research Letters, v. 38, L04302, doi:10.1029/2010GL046227.

Smith, W.H.F., Scharroo, R., Titov, V.V., Arcas, D., and Arbic, B.K., 2005, Satellite altimeters measure tsunami—Early model estimates confirmed: Oceanography, v. 18, no. 2, p. 10–12.

Strasser, M., Moore, G.F., Kimura, G., Kitamura, Y., Kopf, A.J., Lallemant, S., Park, J.O., Screaton, E.J., Su, X., Underwood, M.B., and Zhao, X., 2009, Origin and evolution of a splay fault in the Nankai accretionary wedge: Nature Geoscience, v. 2, p. 648–652, doi:10.1038/ngeo609.

Townend, J., and Zoback, M.D., 2000, How faulting keeps the crust strong: Geology, v. 28, p. 399–402, doi:10.1130/0091-7613(2000)28<399:HFKTCS>2.0.CO;2.

Waldhauser, F., 2009, Near-real-time double-difference event location using long-term seismic archives, with application to northern California: Seismological Society of America Bulletin, v. 99, p. 2736–2748, doi:10.1785/0120080294.

Waldhauser, F., and Schaff, D.P., 2007, Regional and teleseismic double-difference earthquake relocation using waveform cross correlation and global bulletin data: Journal of Geophysical Research, v. 112, B12301, doi:10.1029/2007JB004938.

Weissel, J.K., Anderson, R.N., and Geller, C.A., 1980, Deformation of the Indo–Australian plate: Nature, v. 287, p. 284–291, doi:10.1038/287284a0.

Widiyantoro, S., and Van der Hilst, R.D., 1996, Structure and evolution of the subducted lithosphere beneath the Sunda arc, Indonesia: Science, v. 271, p. 1566–1570, doi:10.1126/science.271.5255.1566.

Manuscript received 5 May 2011
Revised manuscript received 4 October 2011
Manuscript accepted 13 October 2011

Printed in USA